Accounting for buoyancy and ignition influence in the experimental measurement of laminar flame speeds and Markstein lengths from spherical ammonia/air flames

Seif Zitouni, Roman Glaznev, Heinz Pitsch, Joachim Beeckmann, Pierre Bréquigny, Christine Mounaïm-Rousselle, Fabien Halter

▶ **To cite this version:**

Seif Zitouni, Roman Glaznev, Heinz Pitsch, Joachim Beeckmann, Pierre Bréquigny, et al.. Accounting for buoyancy and ignition influence in the experimental measurement of laminar flame speeds and Markstein lengths from spherical ammonia/air flames. Proceedings of the Combustion Institute, 2025, 41, pp.105891. ⟨10.1016/j.proci.2025.105891⟩. ⟨hal-05321897⟩

HAL Id: hal-05321897

https://cnrs.hal.science/hal-05321897v1

Submitted on 6 Jan 2026

HAL is a multi-disciplinary open access archive for the deposit and dissemination of scientific research documents, whether they are published or not. The documents may come from teaching and research institutions in France or abroad, or from public or private research centers.

L'archive ouverte pluridisciplinaire **HAL**, est destinée au dépôt et à la diffusion de documents scientifiques de niveau recherche, publiés ou non, émanant des établissements d'enseignement et de recherche français ou étrangers, des laboratoires publics ou privés.

Distributed under a Creative Commons CC BY-NC-ND 4.0 - Attribution - Non-commercial use - No Derivative Works - International License

Proceedings of the Combustion Institute 41 (2025) 105891

Contents lists available at ScienceDirect

Proceedings of the Combustion Institute

journal homepage: www.elsevier.com/locate/proci

Accounting for buoyancy and ignition influence in the experimental measurement of laminar flame speeds and Markstein lengths from spherical ammonia/air flames

Seif Zitouni [a,b,*], Roman Glaznev [c], Heinz Pitsch [c], Joachim Beeckmann [c], Pierre Bréquigny [a], Christine Mounaïm-Rousselle [a,d], Fabien Halter [a,b]

[a] Université Orléans, INSA CVL, PRISME, UR4229, Orléans, France
[b] CNRS-INSIS, ICARE, 45071 Orléans, France
[c] Institute for Combustion Technology, RWTH Aachen University, 52056 Aachen, Germany
[d] Institut Universitaire de France, IUF, Paris, France

ARTICLE INFO

Keywords:
Ammonia
Laminar burning velocity
Markstein length
Ignition energy
Micro-gravity

ABSTRACT

The burning rate of ammonia/air flames is weak and thereby heavily influenced by buoyancy and radiation introducing large uncertainties in the laminar flame speed determination. Besides, ammonia/air flames exhibit large flame thicknesses and their ignition requires high energy at atmospheric pressure, significantly reducing the radius range for which extrapolation models can be employed to provide accurate unstretched flame speeds. Experiments were conducted using a spherical combustion chamber. The electrical discharge energy was varied until it was insufficient to spark-initiate a self-sustaining flame. Equivalence ratio (ϕ) variations from 0.75 to 1.25 in a pressure range from 1 - 3 bar were investigated. For specific conditions, to eliminate the buoyancy-induced uncertainty, experiments were conducted under micro-gravity. At atmospheric pressure, it has been observed that the initial energy deposit has a strong influence on the duration of the transient phase preceding the self-propagation regime: ammonia/air flames are strongly affected by the initial deposited energy up to a radii of 10 – 15 mm. As the energy is reduced, buoyancy is prompted at smaller flame radii, irrespective of the equivalence ratio. As the pressure increases, the influence of the ignition effect is significantly reduced and disappears after a flame radius of approximately 6 – 8 mm. The study highlights the sensitivity of flame speed and Markstein length to the minimum spark-affected radius selection, particularly under lean conditions. A non-linear trend in Markstein length over the equivalence ratio was observed with a minimum close to $\phi = 0.8 – 0.9$ at similar stretch dependencies for measured experiments in micro-gravity. This trend is in contrast with the quasi-linear relationship reported in the literature, with continuously decreasing Markstein length as conditions get leaner. Finally, the classical adiabatic model showed good agreement with radiation-corrected experimental data, whilst the optically thin model overestimated the influence of radiation for fuel-rich conditions.

1. Introduction

The growing demand for clean energy and transportation solutions to achieve carbon neutrality presents a substantial challenge. Recently, ammonia (NH_3) has gained attention as a carbon-free fuel and energy carrier [1]. However, the combustion characteristics of NH_3, particularly its very low laminar flame speed ($S_L^0 < 10$ cm/s at 298 K and 1 bar), make it highly sensitive to gravitational effects (buoyancy-driven motion) and radiation heat loss, complicating the precise measurement of this fundamental property. Accurate measurements of S_L^0 are essential for validating chemical kinetic models, addressing issues like flashback, blow-off and extinction, and improving turbulent flame interaction in modeling [2].

From the definition of the unstretched laminar flame speed (S_L^0) as the speed at which a planar, unstretched, adiabatic premixed flame propagates relative to the unburned gas [3], various experimental techniques have been developed to measure S_L^0, as reviewed in [4]. Among these, the Spherically Expanding Flame (SEF) method is one of

Article available under the terms of the CC-BY-NC-ND licence (https://creativecommons.org/licences/by-nc-nd/4.0/)
* Corresponding author.
E-mail addresses: seif-eddine.zitouni@univ-orleans.fr, seif.zitouni@cnrs-orleans.fr (S. Zitouni).

https://doi.org/10.1016/j.proci.2025.105891
Received 30 April 2025; Accepted 21 September 2025
Available online 11 October 2025
1540-7489/© 2025 The Authors. Published by Elsevier Inc. on behalf of The Combustion Institute. This is an open access article under the CC BY-NC-ND license (http://creativecommons.org/licenses/by-nc-nd/4.0/).

the most widely used even for NH_3/air flames. A review of the available data reveals significant discrepancies in S_L^0 and corresponding Markstein length (L_b, which represents the sensitivity of a flame to stretch) in the case of NH_3/air flames at normal temperature and pressure (298 K, 1 bar), often exceeding typical measurement uncertainties (see SM, Fig. S.1 and S.2).

In the SEF configuration, flame propagation can be characterized by three distinct phases.

(1) Initially, there is an ignition-dominated phase, where the flame is driven by thermal conduction from the ignition kernel to the reaction front. During this phase, the flame speed and stretch rate increase rapidly. NH_3/air flames exhibit significant flame thickness, requiring higher ignition energy at atmospheric pressure compared to hydrocarbon flames, which may prolong the duration of the ignition-affected regime before transitioning to the quasi-steady regime. For mixtures with large Markstein lengths, such as rich NH_3/air flames [5], strong nonlinear behavior at small radii influences the initial flame transition and the ignition affected radius (r_{min}) [3]. To ensure that the influence of ignition is minimal, a minimum radius is chosen with a value typically set at 6 mm based on CH_4/air simulations [6]. Chen et al. [7] showed from DNS that r_{min} should be estimated depending on the Lewis number (Le), representing the ratio of thermal to mass diffusivity. Although both CH_4 and NH_3/air mixtures exhibit similar thermo-diffusive behavior (Le $\sim$ 1) [5], the distinct intrinsic properties of NH_3 flames (e.g., large ignition energy and flame thickness) may challenge those conclusions.

(2) Once the influence of ignition has dissipated, the flame enters the quasi-steady regime, with stretch decreasing while flame radius is increasing, following the conventional expected behavior [8]. Data from this phase are used to accurately measure flame speed and stretch sensitivity. During this stage, the flow-field of the unburnt gas is assumed to be stationary. However slow-burning flames may challenge the assumption of motionless burned gas due to radiation heat loss and buoyancy induced flow-field [9, 10].

(3) During the final period of the flame evolution, confinement effects, thermal-diffusional instabilities, and buoyancy affect flame propagation and its response to stretch, delimitating the end of the quasi-steady regime. With respect to the slow burning and thermo-diffusional stable NH_3 flame, various methods have been proposed to minimize or correct buoyancy-induced uncertainties. Hayakawa et al. [11] suggested using the ratio of vertical to horizontal radius (r_V/r_H) and flame propagation speed to distinguish the buoyancy-influenced regime from the quasi-steady regime. Other studies [12,13] have relied solely on horizontal radius measurements, but recent DNS [10] and experimental work [14] show this approach is not sufficient to avoid significant errors.

To eliminate buoyancy effects and lengthen the quasi-steady regime phase, experiments in micro-gravity (μg) are justified (e.g., drop towers, parabolic flights). Early work by Ronney [15] investigated NH_3/air flames under free-fall, with the study highlighting challenges in ignition rather than flammability limits. Mathew et al. [14] studied NH_3/air flames using a lab-scale drop tower and found that the buoyancy-induced data distortion could significantly affect the flame propagation and its response to stretch, especially under lean conditions. In addition to buoyancy, radiation heat loss strongly influences slow-burning flames by lowering flame temperature and consequently S_L^0. Several authors have investigated the influence of radiation on NH_3/air flames [16–18]. Glaznev et al. [18] examined the influence of radiation on NH_3/air flames under μg, finding consistent results between optical and pressure-rise data when correcting the first for radiation using the correlation proposed by Yu et al. [19].

Overall, the correct definition of applied radius range for NH_3/air flames remains not clearly stated, which affects the accuracy of flame speed and Markstein length measurements. This may explain the significant discrepancies observed between available literature data. The present study aims to: (1) experimentally determine the spark-affected radius of NH_3/air flames across a broad range of equivalence ratios at both atmospheric and moderately increased pressure (1 – 3 bar); (2) assess whether using a shape-ratio parameter is sufficient to minimize buoyancy-induced uncertainty by comparing static (1 g) and free-fall experiments (μg); (3) compare the measured results with theoretical models, one-dimensional simulations of stationary unstretched flames and transient spherically propagating flames.

2. Experimental framework

2.1. Experimental set-up

Experiments to determine the spark-affected radius of NH_3/air flames were conducted in the spherical constant-volume vessel fully described in [20,21]. This spherical vessel (*1 g configuration*) has an inner diameter of 200 mm and features four orthogonal quartz windows, each 70 mm in size, providing an optical radius access of 35 mm. Microgravity experiments were conducted in ZARM's (Center of Applied Space Technology and Microgravity) GraviTower Bremen providing $<10^{-4}$ g during drops for up to 2.4 s [18]. For the μg experiments, a second well-characterized spherical combustion chamber [22] was used. This vessel (*μg configuration*) has an inner diameter of 100 mm, and optical access with a radius of 25 mm. For both configurations, 1 g and μg, flame propagation was captured using 2 high speed Schlieren imaging systems at 5000 fps and a spatial resolution of $\sim$ 0.1 mm per pixel and 9500 fps and $\sim$ 0.05 mm per pixel, respectively. To ensure accurate comparison between the two spherical vessels and the post-processing methods, first experiments were performed on CH_4/air mixtures (ϕ = 0.9 – 1.2, 298 K, 1 bar). An average difference in S_L^0 was found lower than 3 % between both set-ups. Reference data are available in the supplementary materials (SM).

2.2. Experimental specifications and post-processing methodology

The experiments were first conducted in the 1 g configuration. A spark is generated between two fine electrodes, separated by a fixed spark gap of 3.5 mm, using a standard automotive capacity coil, to allow the adjustment of the deposited spark energy. However, accurate measurement of deposited energy in the gaseous mixture remains challenging due to energy lost to the electrodes through thermal conduction from the generated plasma, voltage drops at the electrodes, and radiation. Previous studies have shown that only 10–25 % of the accumulated discharge energy is converted to thermal energy released to the fuel/air mixture [23]. Therefore, the choice in this study is to refer to the ignition energy in terms of charge duration (E_D), with longer charge durations corresponding to greater deposited energy. Experimental details related to the estimate of the spark energy and methods employed are available in the SM 2.

The electrical charge duration varied from a maximum of 4000 μs, successively decreasing it until the deposited energy was insufficient to maintain a self-sustaining flame. The equivalence ratio (ϕ) was varied from 0.75 – 1.25. For leaner and richer mixture no ignition was achievable with the set-up employed. The influence of pressure at the selected conditions was also investigated from 1 to 3 bar.

The experimental conditions chosen for the μg configuration complemented the experimental database previously reported in [18], using the same set-up and methods. Conditions near the flammability limits of NH_3/air were prioritized (ϕ = 0.7, 1.3), since they are the most difficult to measure under 1 g conditions. A minimum of 2–3 experiments was conducted for each condition. Note that an upper limit was imposed on the exploitable flame radius to ensure that measurements remained

within the constant pressure assumption [3], allowing for a deviation of 3 % in the pressure rise relative to the unburnt pressure. This equates to a maximum radius of ~ 25 and 20 mm, for the 1 g and μg configurations, respectively.

A complete analysis of the uncertainty is provided within the SM for all the conditions summarized in Table 1.

S_L^0 and L_b relative to the burnt side [24], were measured experimentally as described in [5]. The instantaneous effective flame radius (r_{eff}) was calculated by assuming a spherical shape based on the binarized flame contour images, which provide the flame-enclosed area, A, with $r_{eff} = (A/\pi)^{1/2}$. For a SEF, the stretched flame speed (S_b) is defined as the time derivative of the Schlieren flame radius (r_{sch}), $S_b = dr_{sch}/dt$. The flame stretch (K) is expressed as the rate of change of flame area (A), given by $K = (1/A)(dA)/dt = (2/r_{sch})(dr_{sch}/dt)$. The unstretched laminar flame speed with respect to the burnt gas (S_b^0) is determined based on an extrapolation model. For this work, the quasi-steady non-linear relationship (NM-S) between stretched flame speed and stretch proposed by Kelley and Law [8] was used for mixtures with negative L_b, and a model based on flame curvature (LM-C) proposed by Frankel and Sivashinsky [25] for positive L_b, as per the recommendations in [26]. The laminar burning velocity was obtained from the conservation of mass across the flame front with $S_L^0 = \sigma \cdot S_b^0$, with σ the ratio of burnt to unburnt gas densities, evaluated using the 0D equilibrium calculations. A slowly-burning flame may invalidate this relation and the assumption of motionless burned gas due to radiation heat loss, as noted in [14]. Considering the conclusions in Glaznev et al. [18], the radiation correction method proposed by Yu et al. [19] was applied in this study.

2.3. Fundamental theoretical models

The relationships between L_b and Le proposed by Chen and Ju [7,26] and Bechtold and Matalon [27] are considered and compared to experimental results. The first formulation is derived from the analytical developments performed by Chen and Ju, and can be re-arranged to retrieve L_b as per $L_{b\text{-}Chen} = [1/Le - (Ze/2)(1/Le - 1)]\sigma \cdot \delta$, with Ze and δ referring to the Zeldovich number and laminar flame thickness. The second formulation by Bechtold and Matalon was derived from theoretical analysis on the dependence of L_b on stoichiometry, and can be expressed as $L_{b\text{-}BM} = \delta\ [\gamma_1/\sigma - \{(Ze/2)(Le - 1)\gamma_2\}]$, where γ_1 and γ_2 are functions of the expansion ratio, detailed in the SM, alongside methods employed to evaluate the various fundamental flame parameters.

3. Numerical framework

In order to assess various chemical kinetic models, the PREMIX software in the Ansys Chemkin-Pro 2023 package was employed to estimate numerical laminar burning velocities, with multi-component transport accounted for. Four kinetic mechanisms were appraised, NUIG-2023 [28], KAUST-2023 [29], POLIMI-2023 [30] and Han-2020 [31]. The models were selected based on the exhaustive kinetic model evaluation conducted by Girhe et al. [32], with the first three models ranked best overall, whilst Han-2020 was selected due to its performance on laminar burning velocity [32]. Radiation effects were accounted for using the Optically Thin Model (OTM), to evaluate the radiation heat loss from NO, N_2O, NH_3 and H_2O, with Plank-mean coefficients taken from the HITRAN 2008 database [16]. This model does not consider potential reabsorption of heat loss in the burnt gases by the fresh gases. All simulations were also conducted under adiabatic conditions, denoted by ADI. Transient spherically propagating flames were computed using the open-source FlameMaster (FM) program [33]. Isobaric conditions during flame growth are preserved by zero gradient outflow conditions, using a dynamic grid refinement algorithm.

Table 1
Investigated experimental conditions for NH_3/air T_u = 298 K.

Equivalence Ratio (ϕ)	P (bar)	Configuration (μg or 1 g)
0.80,0.85,0.9,1.0,1.05,1.20	1	1 g
1.1,1.3	1	μg
1.1	2	μg – 1 g
0.7,0.9,1.1	3	1 g
0.7,1.1,1.3	3	μg

4. Results and discussion

4.1. Influence of ignition energy

Fig. 1a shows some examples of NH_3/air flame growth for two different timings after ignition with a fixed ignition charge time of 4000 μs at t = 16 and t = 60 ms, respectively. When the charging time (ignition energy) is decreased, mixtures near stoichiometric conditions (ϕ=0.85–1.05) successfully developed into self-sustaining flames, whilst mixtures $0.85 \leq \phi$ and $\phi \geq 1.05$ ignited to form a flame kernel but then extinguished before transition to self-sustained flames.

According to thermal ignition theory [34], the minimum ignition energy (E_{min}) is proportional to the amount of energy needed to heat up a spherical volume of fresh gases with a radius in the same order as the laminar flame thickness (δ_L), from T_u to maximum burnt gas temperature, i.e. T_{ad}, thus $E_{min} \sim \rho_u (\delta_L)^3 c_p (T_{ad} - T_u)$ [2]. Hence, ignition of NH_3/air flames should be more easily achieved at lowest δ_L. Fig. 1(b) illustrates the relationship between the δ_L, the effective Lewis number (Le_{eff}) and E_{min}, with the latter values taken from [35]. E_{min} is located at ~ ϕ = 0.9, whilst minimum δ_L is ϕ = 1.10–1.15. This shift may be attributed to the coupling of positive stretch with preferential diffusion (Le_{eff}), since positive stretch weakens the expanding ignition kernel when Le_{eff} exceeds unity (ϕ > 1, Fig. 1b), the critical ignition radius increases (thus E_{min}) even though δ_L is smaller. This emphasizes the importance of the thermal and mass balance across the flame front of the developing flame kernel [36]. For lean NH_3/air flames the δ_L is large, while for rich flames Le > 1 hinders flame kernel expansion, hence the challenges in achieving self-sustained flames for off-stoichiometric conditions. Figueroa-Labastida et al. [37] and Verkamp et al. [38] reported similar findings, noting that ignition was most difficult under rich conditions, followed by lean and then stoichiometric cases.

Fig. 2b illustrates the temporal evolution of an NH_3/air flame (ϕ = 1.1, 2 bars) at different charge time, alongside the flame morphology at t = 60 ms (Fig. 2a). It is observed that decreasing the ignition energy results in a longer initial non-linear phase prior to a fairly linear transition. While this behavior is typical for all spherical flames [8,36], it is more pronounced in NH_3/air flames due to the low flame speed, which leads to significant changes in the flame shape. A clear departure from circularity, quantified by the vertical-to-horizontal radius ratio (r_V/r_H), is evident in Fig. 2a and further corroborated by the evolution of the sphericity ratio in Fig. 2b as ignition energy decreases. Under these conditions, buoyancy influences the flame at progressively smaller radii, ultimately given rise to the characteristic mushroom head morphology. As a result, the transition from quasi-steady regime propagation to the buoyancy-dominated regime is shortened or, in some cases, entirely suppressed, thereby constraining the radius range available for reliable extrapolation.

In their DNS study, Berger et al. [10] attributed the observed flame shape to variations in the flow field. Furthermore, when the flame front does not develop an acute cusp and non-unity Le effects are negligible, the displacement speed remains proportional to both the strain and curvature, with extrapolation to zero-stretch introducing an error of 3 % - with this approach employed in previous studies [37]. In practice, ignition energies close to E_{min} are often chosen to minimize the initial ignition effects. However, for NH_3/air flames, this significantly impacts flame morphology and, in some instances, induces early buoyancy effects. On the other hand, excessive energy deposit can result in over-driving flame propagation ('false' non-buoyant flames) – thereby underscoring the necessity of carefully controlling ignition. As such, it

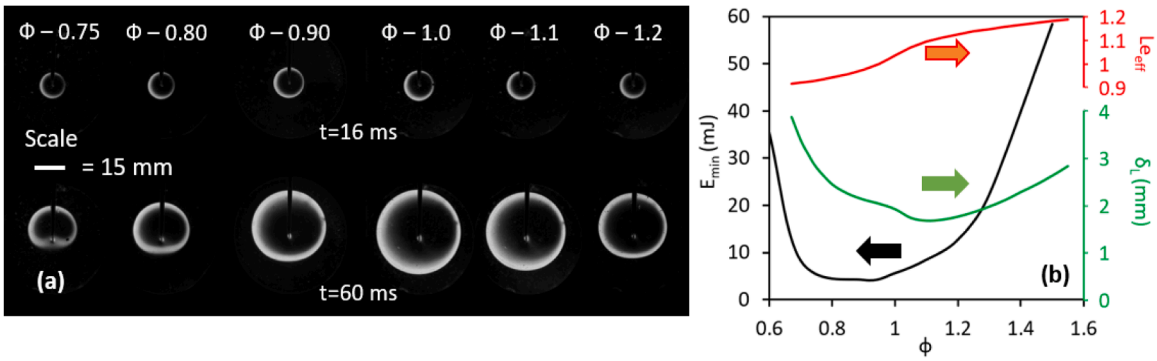

Fig. 1. (a) Schlieren images at time $t = 16$ and $t = 60$ ms after ignition, (b) E_{min}, Le_{eff} and δ_L as a function of ϕ (298 K, 1 bar).

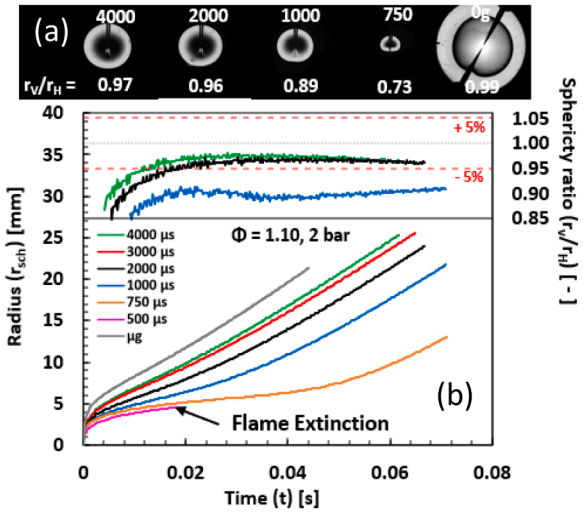

Fig. 2. (a) Flame image, 60 ms after spark discharge timing, (b) Temporal evolution of NH_3/air flame with different charge durations (µs).

seems crucial to incorporate a parameter that characterizes the sphericity of the NH_3/air SEF during data processing to maintain the assumption of a spherical shape, especially when the Richardson number – comparing the characteristic time scale of flame propagation to that of buoyancy convection – exceeds unity [10,14], which is typically the case for NH_3/air flames. To this end, a 5 % sphericity threshold was applied during data processing to define the upper radius limit used for extrapolation, thereby obviating the need for aspherical corrections. The temporal evolution of the sphericity ratio for all cases is provided in the SM.

Fig. 3 shows the change in S_b and stretch rate, K, at $\phi = 1.1$ and two pressures (1 and 3 bar) by considering experimental data when $r_V/r_H \geq 0.95$, to minimize uncertainty related to buoyancy-effects. In all cases ($\phi = 0.9$ is located in the SM), the lower the charging time (ignition energy), the more pronounced the non-linear transition between ignition-affected and quasi-steady regimes. At 1 bar, all flame trajectories converge at a radius ~ 14 mm, at which point they lie within the experimental uncertainty of one another. This minimum radius is notably larger than those of CH_4/air flames (~ 6 mm) [6]. It reduces the number of individual points that will be considered for the extrapolation optimization to extract the unstretched flame speed. When the pressure is increased to 3 bar, the non-linear transition is replaced by a much more linear progression, in agreement with DNS work [35], with the critical ignition radius reducing to ~ 8 mm for $\phi = 1.1$. Chen et al. [7] showed that this critical ignition radius is Le dependent but CH_4 and NH_3 exhibit very similar thermo-diffusive properties (at $\phi = 1.1$, Le_{eff} ~ 1.05 and 1.09, respectively). As an increase in pressure leads to a reduction in flame thickness whilst Le remains unaffected, the variation in critical ignition radius is primarily influenced by changes in flame thickness. All critical ignition radii measured for all conditions in this study can be found in the SM (Table S.1), ranging from ~10 to 15 mm for $\phi = 0.80$ and 1.20, respectively, at 1 bar.

Complementary experiments were conducted under µg conditions to evaluate the buoyancy effect, as plotted in Fig. 3. The same methods of data-processing and extrapolation were employed to all datasets. At 1 bar, the µg experiment exhibits similar flame speed, stretch dependency, and critical ignition radius with the 1 g experiments. However, at 3 bar,

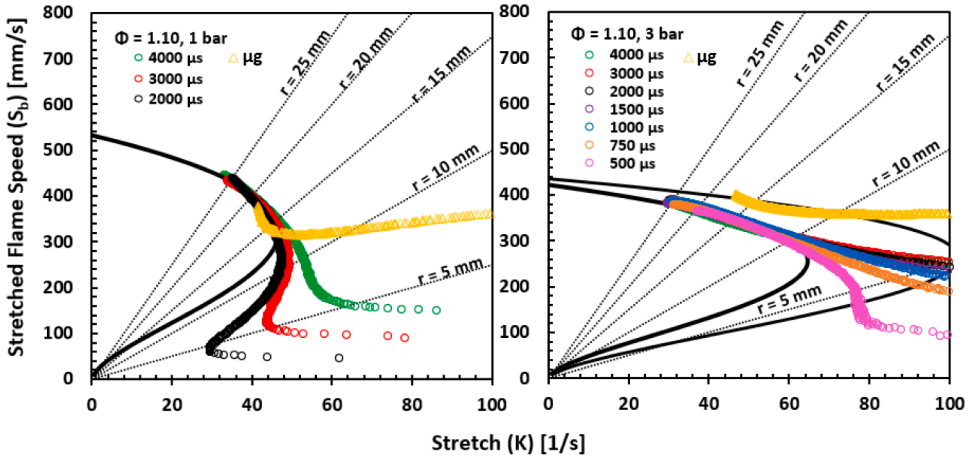

Fig. 3. Effect of charge duration (µs) on propagation of SEF NH_3/air flames at 1 and 3 bars for 1 g (circles) and µg (triangles). The solid black line represents the NM-S extrapolation model [8], fitted for 2000 µs case for the 1 g experiments.

the S_b evolution as a function of K is strongly different, with a substantial increase in S_b for a fixed stretch rate compared to the 1 g configuration. This behavior has been observed in recent experiments [14] and DNS [10], and is caused by the local buoyancy-induced flow in the 1 g case.

A sensitivity analysis was performed on the selection of r_{min} for experiments conducted at 1 bar, by reducing the experimental r_{min} value by 1 to 3 mm for a wide range of ϕ. Noteworthily, the stretch dependency of the lean flames changed with r_{min} for ϕ = 0.8–0.85, from a positive to negative L_b, underlining how sensitive NH_3/air flames are to the r_{min} selection, as illustrated in Fig. 4. The leanest flame (ϕ = 0.8) showed the most sensitivity to the choice of r_{min}, with differences in extrapolated S_b^0 ~11 % and 33 % for reductions of 1 and 3 mm, respectively.

4.2. Laminar burning velocity and Markstein length

The laminar burning velocity (S_L^0) and corresponding Markstein lengths (L_b) measured in this study, both in 1 g and μg configuration are plotted in Fig. 5. The radiation was taken into account using the correlation proposed by Yu et al. [19]. Experimental data from literature [11,14,18,37,39–42], numerical simulations and theoretical values are also plotted. Of the appraised reaction mechanisms, only NUIG 2024 and KAUST 2023 models are plotted, as they consistently showed the best agreement with the present measurements. For the results from computing unsteady spherical flames with NUIG 2024 and using the same extrapolation procedure as for the experiments (denoted as FM), the same range of radii was selected as in the experiments to ensure consistency with the present measurements. The theoretical values (L_b-Chen and L_b−Matalon) are also based on the NUIG 2024 model. All the reaction mechanisms evaluated gave the same qualitative trends, with the full data sets available in the SM.

As can be seen from Fig.5a, at 1 bar, very good agreement is observed between 1 g from this study and free-fall tests, including recent μg experiments conducted by Mathew et al. [14]. The ADI model provides good agreement with radiation-corrected experimental results [14,18]. When data is not corrected for radiation [11,39,40], the OTM model shows better agreement under lean conditions than under rich conditions, where it underestimates the impact of radiation. The results using the SEF method yields significantly higher S_L^0 than the heat-flux (H.F) configuration [39], even though the H.F set-up should theoretically be buoyancy-free. At 3 bar, Fig 5.b, although data is limited, good agreement is witnessed between the μg experiments and the reaction mechanisms. At ϕ = 0.7, 1 g S_L^0 is significantly higher from the 1 g configuration than the μg one, which may be due to the limited radii range available due to buoyancy triggered at very small flame radii, increasing extrapolation uncertainty. Results from FM with OTM show best agreement with measurements from Hayakawa et al. [11], which were not corrected for radiation.

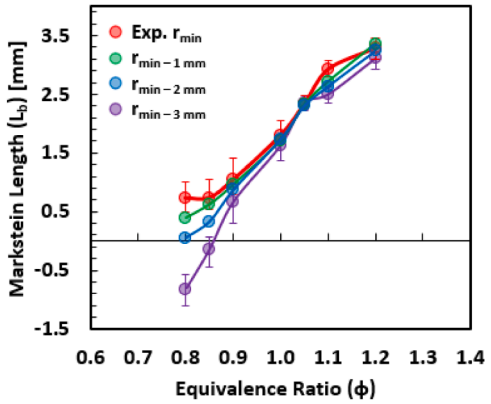

Fig. 4. Influence of r_{min} choice on L_b for NH_3/air flames.

Markstein lengths (L_b) are illustrated in Fig. 5c at 1 bar. It should be noted that very limited datasets of L_b are available in the literature. Both 1 g and μg tests conducted in this study exhibit similar L_b across ϕ = 0.80 – 1.2. However, an inflection point is observed for the μg tests between ϕ = 0.8 – 0.9, with L_b increasing with decreasing ϕ. This behavior could not be verified experimentally at 1 g due to buoyancy, but a plateau in L_b is observable for ϕ = 0.80 – 0.85. Qu et al. [35] numerically estimated L_b, observing a similar non-linear trend to that of the μg tests.

The positive L_b in this study for lean mixtures are opposite to the negative L_b values measured in [5,11], at ϕ = 0.8 – 0.9. As discussed previously, NH_3/air flames exhibit a high sensitivity to the choice of r_{min} under lean conditions, with r_{max} being highly dependent on E_{ign}, leading to a significant change in the flame stretch sensitivity prediction. Moreover, it is worth noting that none of the theoretical models predict a negative L_b, nor an increase in L_b at leanest conditions. Regarding the L_b estimates using FM, both the ADI and OTM model show good agreement with the measured 1 g results, except at ϕ = 0.8 when OTM is considered.

An increase in pressure results in a change in stretch-sensitivity under lean conditions as illustrated in Fig. 5d This is largely due to an increase in hydrodynamic instability due to reduced flame thickness and increased expansion ratio rather than an increase in thermo-diffusional instabilities (as Le and the Ze exhibit very little change, see SM). While the theoretical models predict a decrease in L_b with an increase in pressure, they are unable to predict the change in stretch sensitivity behavior observed under lean conditions. The ADI model shows best agreement with radiation uncorrected L_b, whereas the OTM model significantly overestimates the measured decrease in L_b under lean conditions.

Given the good agreement between the 1 g and μg experiments, it suggests that enforcing a parameter to define flame sphericity (r_V/r_H) could help limit buoyancy-related uncertainty to some extent, provided it is applied rigorously, combined with r_{min} selection. However, a broader test matrix would need to be evaluated to further validate this approach against μg results.

5. Conclusions

New experiments were conducted both in 1 g and μg conditions using the SEF configuration to investigate the spark-affected radius of NH_3/air flames from lean to rich conditions and up to 3 bar. The results show that when the ignition is as low as possible to guarantee the self-sustainability of the initial flame kernel, NH_3/air flames exhibit a pronounced non-linear transition from ignition to quasi-steady propagation, with the flame shape influenced by buoyancy at smaller radii, especially in rich conditions. The critical ignition radius that has to be considered to perform extrapolation in the self-sustained regime for NH_3/air flames is notably larger compared to CH_4/air flames. Differences can be primarily attributed to variations in flame thickness rather than Lewis number. The sensitivity of the unstretched flame speed and Markstein length to the minimum critical radius selection, especially in lean conditions (φ = 0.8 – 0.85) and ambient pressure, underlines the need for careful data processing to minimize uncertainty. The experiments in μg configurations confirm the results observed under terrestrial gravity, with both exhibiting similar non-linear stretch behavior at ambient pressure. The OTM model which takes into account species radiation overestimates the value of the Markstein length compared to classical adiabatic assumption particularly at lean conditions, for the appraised reaction mechanisms. Finally, fundamental theoretical models were appraised, showing qualitative agreement at 1 bar, but unable to capture the change in Markstein length at higher pressures requiring further analysis. These findings underscore the need for more comprehensive modeling and careful choice of data-processing range to accurately predict NH_3/air flame dynamics.

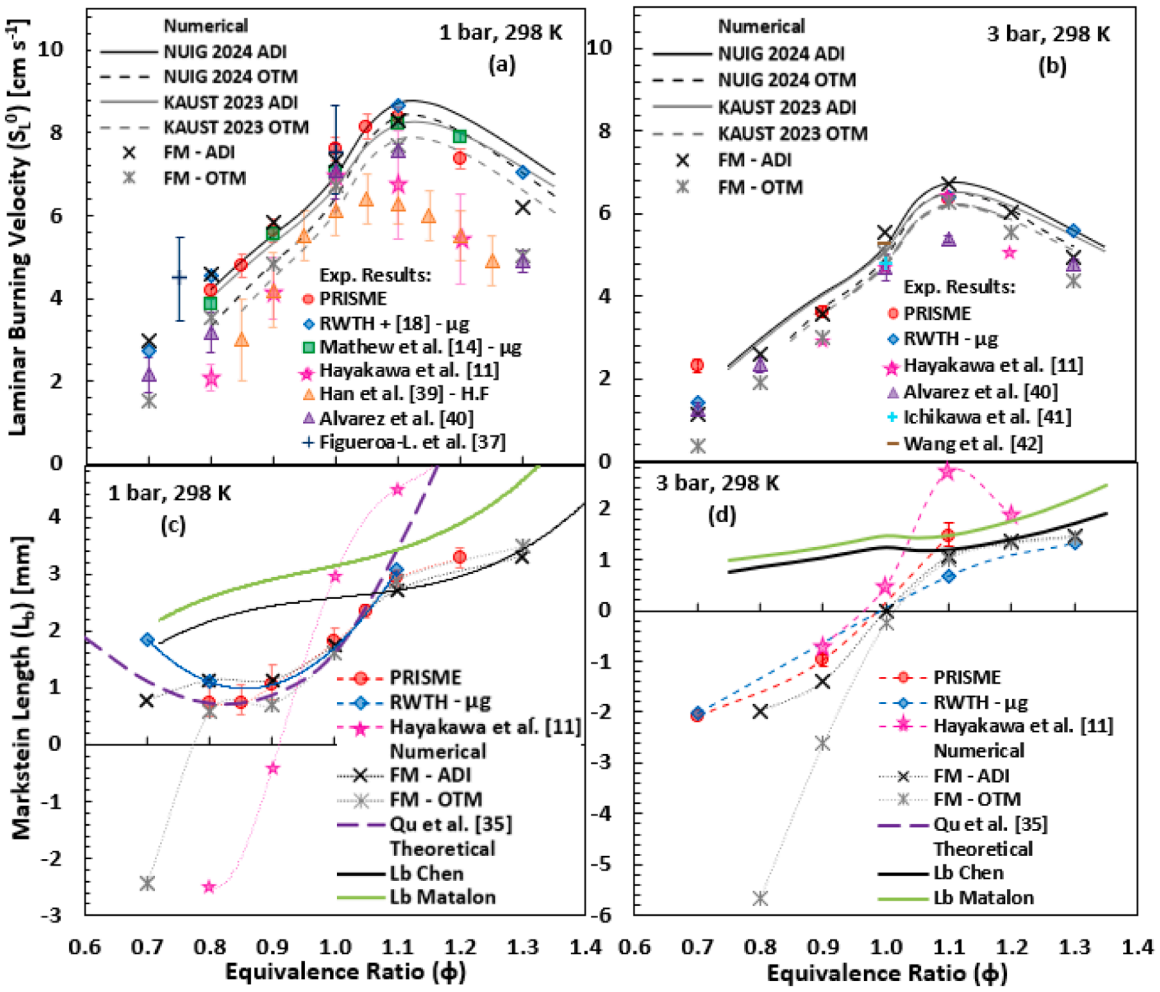

Fig. 5. S_L^0 of NH_3/air flames at (a) 1 bar and (b) 3 bars, alongside L_b of NH_3/air flames at (c) 1 bar and (d) 3 bars.

Novelty and significance statement

Ammonia/air flames require high ignition energy at atmospheric pressure, and their low burning velocity is significantly affected by buoyancy and radiation. These factors limit the applicable data post-processing range and introduce considerable uncertainty in determining laminar flame speeds. The novelty of this research is to experimentally quantify the effect of ignition energy on early ammonia/air flame propagation, across a broad range of equivalence ratios, at ambient temperature, and up to moderate pressures (3 bar), with critical ignition radii determined for the first time. Furthermore, a flame sphericity parameter was validated by comparing measurements under normal gravity (1 g) and microgravity (µg), helping to minimize buoyancy-related uncertainties. Radiation-corrected flame speeds measured under both gravity conditions were compared with theoretical models, one-dimensional simulations of stationary unstretched flames, and transient spherically expanding flames. The findings highlight the importance of robust modeling and careful selection of the data-processing range to accurately capture the behavior of NH_3/air flames, especially under lean conditions where improper handling can yield erroneous assessment of stretch-sensitivity.

Declaration of competing interest

The authors declare that they have no known competing financial interests or personal relationships that could have appeared to influence the work reported in this paper.

Acknowledgements

The authors gratefully acknowledge the financial support from ANR-11-LABX-0006-01 and ANR-22-CE50-0022, as well as the support of Deutsche Forschungsgemeinschaft (DFG, German Research Foundation, Germany), Grant No 469834263, and the European Space Agency (ESA) for funding the drops and the Center of Applied Space Technology and Microgravity (ZARM), Germany for providing the drops in the Grav-iTower Bremen. Moreover, the present work has received the support of the Research Program “Micropesanteur fondamentale et appliquée”, GDR CNRS No.2799.

Supplementary materials

Supplementary material associated with this article can be found, in the online version, at doi:10.1016/j.proci.2025.105891.

References

[1] W.S. Chai, Y. Bao, P. Jin, G. Tang, L. Zhou, A review on ammonia, ammonia-hydrogen and ammonia-methane fuels, Renew. Sustain. Energy Rev. 147 (2021) 111254.
[2] C.K. Law, Combustion Physics, Cambridge University Press, 2006.
[3] Z. Chen, On the accuracy of laminar flame speeds measured from outwardly propagating spherical flames: methane/air at normal temperature and pressure, Combust. Flame 162 (2015) 2442–2453.
[4] F.N. Egolfopoulos, et al., Advances and challenges in laminar flame experiments and implications for combustion chemistry, Prog. Energy Combust. Sci. 43 (2014) 36–67.

[5] S. Zitouni, P. Brequigny, C. Mounaïm-Rousselle, Influence of hydrogen and methane addition in laminar ammonia premixed flame on burning velocity, Lewis number and Markstein length, Combust. Flame 253 (2023) 112786.
[6] D. Bradley, P.H. Gaskell, X.J. Gu, Burning velocities, Markstein lengths, and flame quenching for spherical methane-air flames: a computational study, Combust. Flame 104 (1996) 176–198.
[7] Z. Chen, M.P. Burke, Y. Ju, Effects of Lewis number and ignition energy on the determination of laminar flame speed using propagating spherical flames, Proc. Combust. Inst. 32 (2009) 1253–1260.
[8] A.P. Kelley, C.K. Law, Nonlinear effects in the extraction of laminar flame speeds from expanding spherical flames, Combust. Flame 156 (2009) 1844–1851.
[9] C.K. Law, G.M. Faeth, Opportunities and challenges of combustion in microgravity, Prog. Energy Combust. Sci. 20 (1994) 65–113.
[10] L. Berger, et al., A DNS study of the impact of gravity on spherically expanding laminar premixed flames, Combust. Flame 216 (2020) 412–425.
[11] A. Hayakawa, et al., Laminar burning velocity and Markstein length of ammonia/air premixed flames at various pressures, Fuel 159 (2015) 98–106.
[12] Y. Li, M. Bi, B. Li, W. Gao, Explosion behaviors of ammonia-air mixtures, Combust. Sci. Technol. 190 (2018) 1804–1816.
[13] U.J. Pfahl, M.C. Ross, J.E. Shepherd, K.O. Pasamehmetoglu, C. Unal, Flammability limits, ignition energy, and flame speeds in H2-CH4-NH3-N2O-O2-N2 mixtures, 2000.
[14] J. Mathew, J.K. Tavares, J. Jayachandran, Accurately measuring slowly propagating flame speeds: application to ammonia/air flames, Combust. Flame 271 (2025) 113807.
[15] P.D. Ronney, Effect of chemistry and transport properties on near-limit flames at microgravity, Combust. Sci. Technol. 59 (1988) 123–141.
[16] H. Nakamura, M. Shindo, Effects of radiation heat loss on laminar premixed ammonia/air flames, Proc. Combust. Inst. 37 (2019) 1741–1748.
[17] M. Faghih, A. Valera-Medina, Z. Chen, A. Paykani, Effect of radiation on laminar flame speed determination in spherically propagating NH3-air, NH3/CH4-air and NH3/H2-air flames at normal temperature and pressure, Combust. Flame 257 (2023) 113030.
[18] R. Glaznev, et al., Ultra-slow ammonia flame speeds — A microgravity study on radiation, Proc. Combust. Inst. 40 (2024) 105334.
[19] H. Yu, et al., Radiation-induced uncertainty in laminar flame speed measured from propagating spherical flames, Combust. Flame 161 (2014) 2815–2824.
[20] B. Galmiche, F. Halter, F. Foucher, Effects of high pressure, high temperature and dilution on laminar burning velocities and Markstein lengths of isooctane/air mixtures, Combust. Flame 159 (2012) 3286–3299.
[21] C. Lhuillier, P. Brequigny, N. Lamoureux, F. Contino, C. Mounaïm-Rousselle, Experimental investigation on laminar burning velocities of ammonia/hydrogen/air mixtures at elevated temperatures, Fuel 263 (2020) 116653.
[22] R. Hesse, et al., Elucidating the challenges in extracting ultra-slow flame speeds in a closed vessel—A CH2F2 microgravity case study using optical and pressure-rise data, Proc. Combust. Inst. 39 (2023) 1783–1792.
[23] K. Eisazadeh-Far, F. Parsinejad, H. Metghalchi, J.C. Keck, On flame kernel formation and propagation in premixed gases, Combust. Flame 157 (2010) 2211–2221.
[24] D. Dunn-Rankin, F. Weinberg, Location of the Schlieren image in premixed flames: axially symmetrical refractive index fields, Combust. Flame 113 (1998) 303–311.
[25] M.L. Frankel, G.I. Sivashinsky, On effects due to thermal expansion and lewis number in spherical flame propagation, Combust. Sci. Technol. 31 (1983) 131–138.
[26] Z. Chen, On the extraction of laminar flame speed and Markstein length from outwardly propagating spherical flames, Combust. Flame 158 (2011) 291–300.
[27] J.K. Bechtold, M. Matalon, The dependence of the Markstein length on stoichiometry, Combust. Flame 127 (2001) 1906–1913.
[28] Y. Zhu, et al., The combustion chemistry of ammonia and ammonia/hydrogen mixtures: a comprehensive chemical kinetic modeling study, Combust. Flame 260 (2024) 113239.
[29] X. Zhang, K.K. Yalamanchi, S.Mani Sarathy, Combustion chemistry of ammonia/C1 fuels: a comprehensive kinetic modeling study, Fuel 341 (2023) 127676.
[30] A. Stagni, et al., Low- and intermediate-temperature ammonia/hydrogen oxidation in a flow reactor: experiments and a wide-range kinetic modeling, Chem. Eng. J. 471 (2023) 144577.
[31] X. Han, et al., The temperature dependence of the laminar burning velocity and superadiabatic flame temperature phenomenon for NH3/air flames, Combust. Flame 217 (2020) 314–320.
[32] S. Girhe, et al., Ammonia and ammonia/hydrogen combustion: comprehensive quantitative assessment of kinetic models and examination of critical parameters, Combust. Flame 267 (2024) 113560.
[33] H. Pitsch, Flamemaster: a C++ computer program for 0D combustion and 1D laminar flame calculations, 1998.
[34] B. Lewis, G. Von Elbe, Combustion, Flames and Explosions of Gases, Academic Press, New York, 1961.
[35] Z. Qu, Y. Wang, X. Chen, Z. Chen, Effects of partial fuel cracking on the forced ignition and spherical flame propagation in ammonia/air mixtures, Fuel 378 (2024) 132936.
[36] D. Yu, Z. Chen, Premixed flame ignition: theoretical development, Prog. Energy Combust. Sci. 104 (2024) 101174.
[37] M. Figueroa-Labastida, et al., Shock-tube laminar flame speed measurements of ammonia/airgon mixtures at temperatures up to 771 K, Combust. Flame 260 (2024) 113256.
[38] F.J. Verkamp, M.C. Hardin, J.R. Williams, Ammonia combustion properties and performance in gas-tubrine burners, Symp. (Int.) Combust. 11 (1967) 985–992.
[39] X. Han, et al., Experimental and kinetic modeling study of laminar burning velocities of NH3/air, NH3/H2/air, NH3/CO/air and NH3/CH4/air premixed flames, Combust. Flame 206 (2019) 214–226.
[40] L.F. Alvarez, J. Shaffer, C.E. Dumitrescu, O. Asakari, Laminar burning velocity of Ammonia/air mixtures at high pressures, Fuel 363 (2024) 130986.
[41] A. Ichikawa, et al., Laminar burning velocity and Markstein length of ammonia/hydrogen:air premixed flames at elevated pressures, Int. J. Hydrogen Energy 40 (2015) 9510–9578.
[42] S. Wang, et al., Experimental study and kinetic analysis of the laminar burning velocity of NH3/syngas/air, NH_3/CO/air and NH_3/H_2/air premixed flames at elevated pressures, Combust. Flame 211 (2020) 270–287.